Supporting Information for

On the patterns and scaling properties of the 2021-2022 Arkalochori earthquake sequence (Central Crete, Greece) based on Seismological, Geophysical and Satellite observations.

Filippos Vallianatos [1,2] , Andreas Karakonstantis[1,2], Georgios Michas[1,2] , Kyriaki Pavlou[1,2] , Maria Kouli[1,3] , Vassilis Sakkas[1,2]

[1]Section of Geophysics–Geothermics, Department of Geology and Geoenvironment, National and Kapodistrian University of Athens, 15784 Zografou, Athens, Greece

[2]Institute of Physics of the Earth's Interior and Geohazards, UNESCO Chair on Solid Earth Physics and Geohazards Risk Reduction, Hellenic Mediterranean University Research Center (HMURC), GR 73133, Chania, Crete, Greece.

[3]Hellenic Mediterranean University, Faculty of Electronic Engineering, Romanou 3, Chania, Crete, Greece

Contents of this file

Introduction

This supporting information provides more information on the methods, additional figures and tables used in the main article.

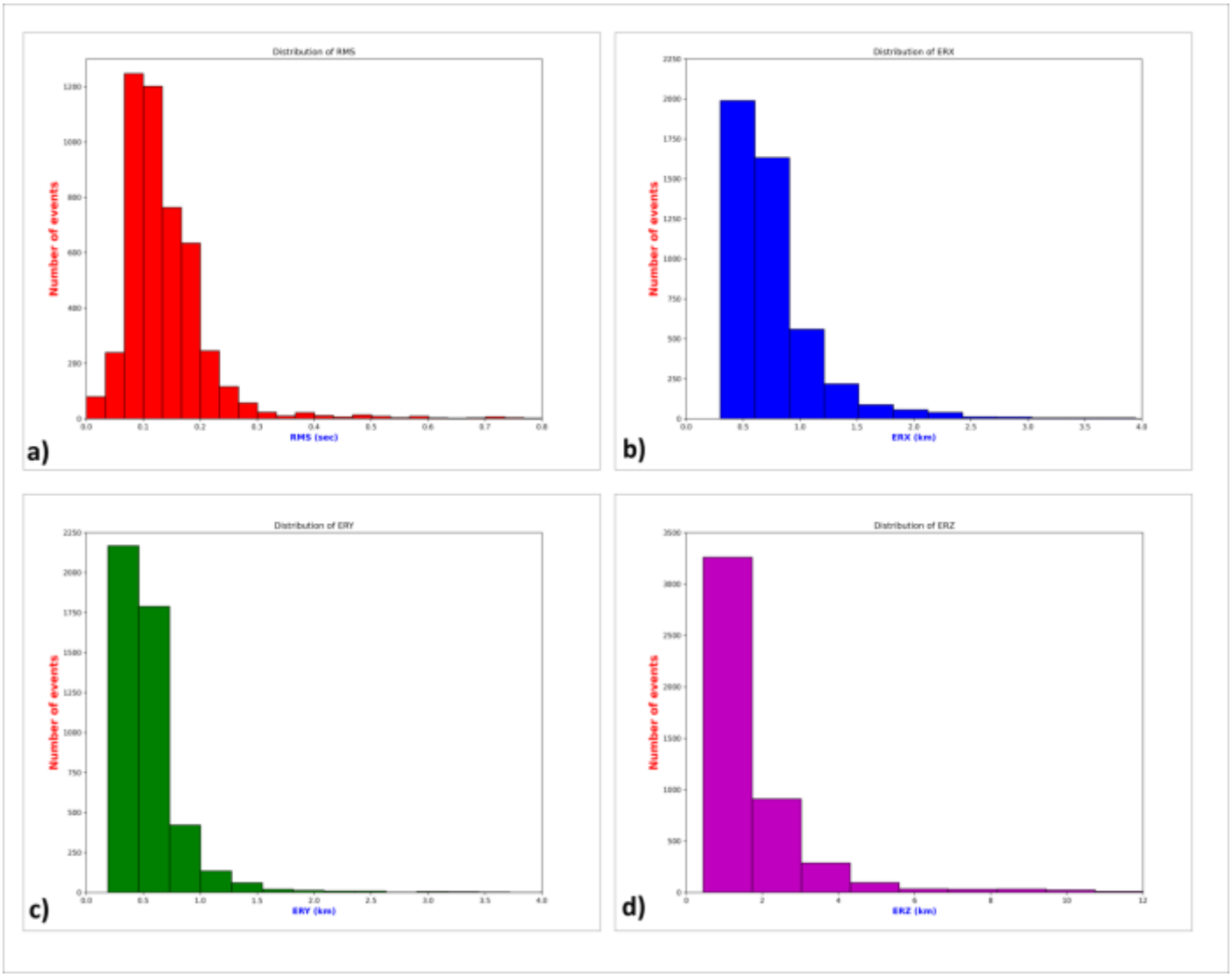

Figure S1 Statistics of the (a) RMS (b) X-horizontal location error (ERX) (c) Y-horizontal location error (ERY) (d) Z-vertical location error (ERZ)

Travel-time Tomography-Synthetic tests

P- and S-phases of more than 800 events, recorded during the 2021-2022 time period by local and regional stations of the Hellenic Unified Seismological Network (HUSN) and the Hellenic Strong Motion Network (HSMN), located in Southern Greece, were used for the tomographic inversion. Synthetic tests were performed to set the input parameter values that produced better resolution and increased the fidelity area. Regarding the 3-D tomographic inversion, a dataset consisting of 12,236 P- and 9,820 S-arrival-times was selected, with at least 12 phases per event (Supplementary material, Figure S2). The algorithm provides two alternative options: inversion for V_P and V_S (V_P–V_S scheme) using P and S travel-time residuals (dt_P and dt_S) and inversion for V_P and V_P/V_S ratio (V_P–V_P/V_S scheme) using dt_P and differential residuals, $dt_S - dt_P$. In this study, inversion was performed for both V_P–V_S and V_P–V_P/V_S schemes, in order to obtain

additional constraints concerning the V_P and V_S anomalies (Koulakov 2009; Jaxybulatov et al. 2011).

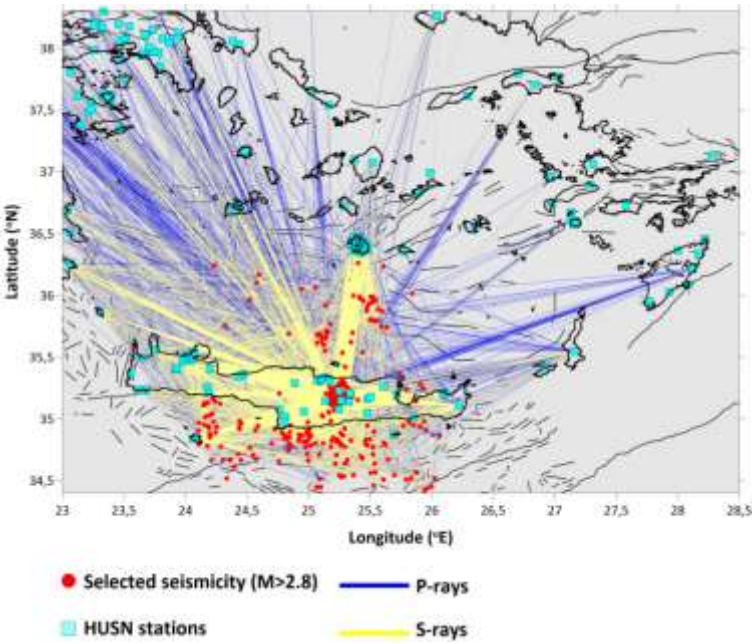

Figure S2 Total P- (blue) and S-ray (yellow) distribution. Red triangles indicate locations of the HUSN and the HSMN stations. The selected seismicity (M≥2.8) during the study period (2021-2022) is presented by red circles.

Sensitivity analysis

In this study, sensitivity analysis for the available dataset was performed by applying the checkerboard test (Humphreys and Clayton 1988). This method uses alternating anomalies of fast and slow velocity perturbations, relative to the initial 1-D gradient model, evenly spaced throughout the model, in a checkerboard pattern (Figures S3-S4). The data resolution is mainly controlled by the ray-path distribution, the model parameterization and smoothing (Lees and Crosson 1989). The average spacing between stations is of the same order as the minimum size of the resolved anomalies in the tomographic inversion (Koulakov and Shapiro 2015).

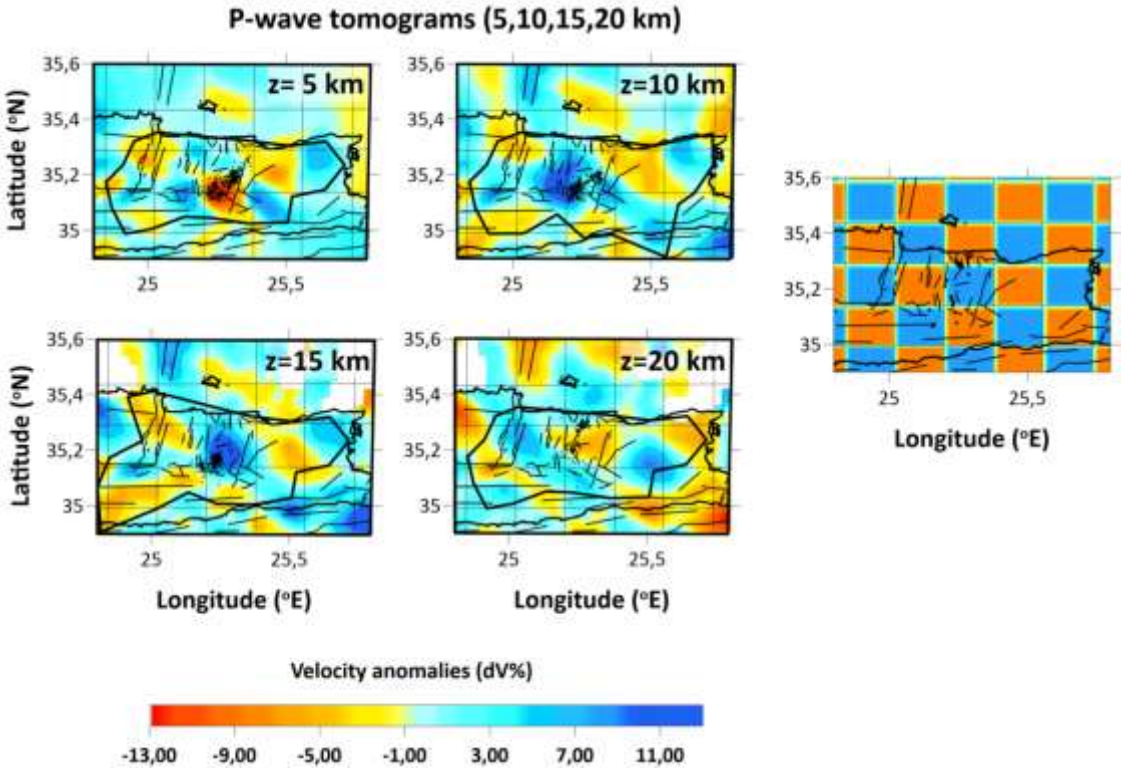

Figure S3 Reconstruction of P-wave anomalies for the depth slices of 5, 10, 15 and 20 km with anomaly cell size of 10×10 km^2. The confidence area is included within the dashed-outline polygon.

Checkerboard tests are performed to reproduce the attributes of the real data processing procedure. In the initial synthetic models, the size of cells corresponds to the expected anomalies. The applied procedure requires the definition of spiked regions, with 10% variability in the velocity structure, compared to the reference 1-D velocity model. Travel-times for the paths between the source and the receiver were computed. Subsequently, random noise was added to the synthetic travel-time residuals, to resemble the respective RMS errors of 0.18 s for P-waves and 0.21 s for S-waves which are observed in the real-data. This procedure corresponds to the real observation system, which uses 3-D ray tracing that follows the bending algorithm principles. The reconstruction of the synthetic model is performed in the same way as with the real data processing, including the 1-D velocity model optimization and the absolute source location. After performing several synthetic tests, the set of parameters that provided a greater confidence area and could successfully reconstruct the model of checkerboard anomalies was used for the 3-D tomographic inversion, using real data. The inversion variance is controlled by errors in the data, including mis-picks, mislocations and incorrectly determined ray-paths.

An example of a checkerboard test, presented herein, consists of alternating 10x10 km^2 anomalies for the horizontal tests, which define the limitations of our model. The variations (%) of body-wave velocity anomalies (±13%) are presented in Figures S3-S4, at depths of 5, 10, 15, and 20 km. The sign of the velocity is changed at 5 and 15 km depth, in order to check the vertical resolution. The synthetic model is reconstructed relatively well within the region between Heraklion basin to the north and Asterousia mountains to the south 35.00ºN-35.25ºN, 24.90ºE-25.60ºE). More specifically, the anomalies do not resolve well within the depth slices of

10 km and 15 km depth for either of the P- and S-wave velocity models. Horizontal smearing is observed towards the northern and the western part of the study area, mainly due to the azimuthal gap of the available seismological stations and the absence of significant seismic activity recorded during the study period.

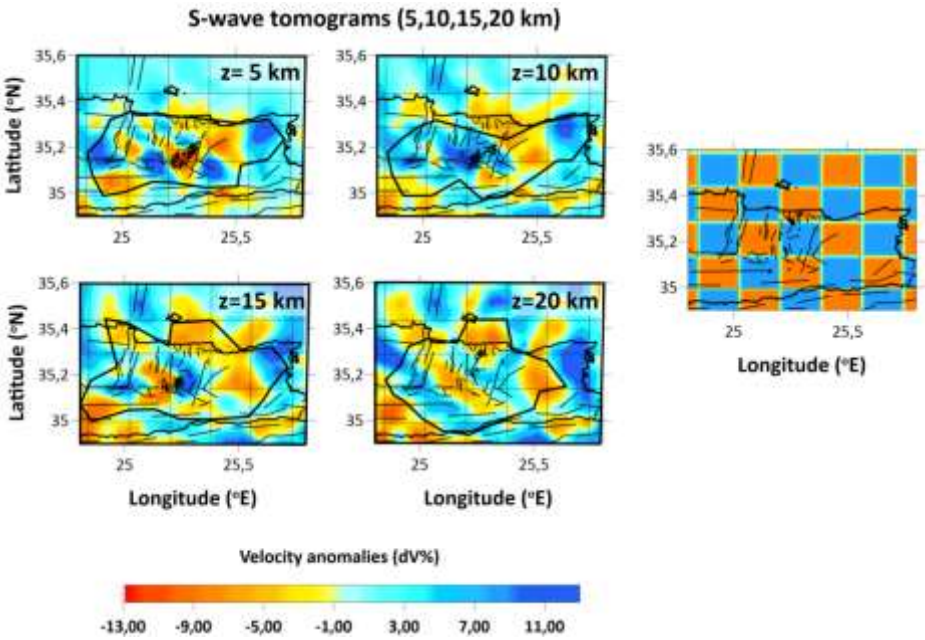

Figure S4 Reconstruction of S-wave anomalies for the depth slices of 5, 15, 20, and 25 km with anomaly cell size of 10×10 km^2. The confidence area is included within the dashed-outline polygon.

Synthetic tests showed that the absolute amplitudes of the body-wave anomalies were up to 5% smaller than the respective ones off or the starting checkerboard grid. These tests are used as a preliminary tool to understand whether the ray configuration enables the reconstruction of the shape of small patterns at all depths. In the case where this condition is not fulfilled, the results of the tests indicate the size of the anomaly preserved throughout the examined depth interval. The size and form of the resolved area for the horizontal slices, in combination with the presence of dense ray coverage for the horizontal slices, provide reliability to the interpretation of the final results of the velocity perturbations.

GNSS data and results

Time series of the stations coordinates were formed for the four continuous GNSS stations operated on the broad area of central-eastern Crete. The velocity vector was estimated for the period prior to the strong seismic event on September 2021, and for the period followed that event. Sites MOI1 and IERA have shown insignificant or no co-seismic displacement and therefore only one velocity vector is presented for the indicated time period.

Table S1. Velocity components for the four continuous GNSS stations on the central-eastern part of Crete.

Site	Latitude(°)	Longitude (°)	Period	V_{East} (mm/yr)	V_{North} (mm/yr)	V_{Up} (mm/yr)
ARKL	35.1339	25.2689	Jan. 30, 2017 - Sept. 26, 2021 4.66yrs	7.20 ± 0.04	-15.02 ± 0.05	-0.88 ± 0.09
			Sept. 29, 2021 – Apr. 30, 2022 0.59yrs	4.76 ± 0.73	-19.85 ±0.80	-26.78 ± 2.56
HERA	35.4241	25.1415	Dec. 2, 2013 - Sept. 26, 2021 7.82yrs	7.96 ± 0.02	-13.54 ± 0.02	-0.56 ± 0.05
			Sept. 29, 2021 – Apr. 30, 2022 0.59 yrs	4.93 ± 0.65	-5.62 ± 0.62	9.81 ± 1.80
MOI1	35.0503	24.8719	May 1, 2020 – Apr. 30 2022 2.00yrs	6.62 ± 0.11	-17.62 ± 0.14	-3.72 ± 0.40
IERA	35.0530	25.7970	Jul.5, 2011 – Apr. 30 2022 10.83yrs	9.14 ± 0.02	15.02 ± 0.03	-0.85 ± 0.05

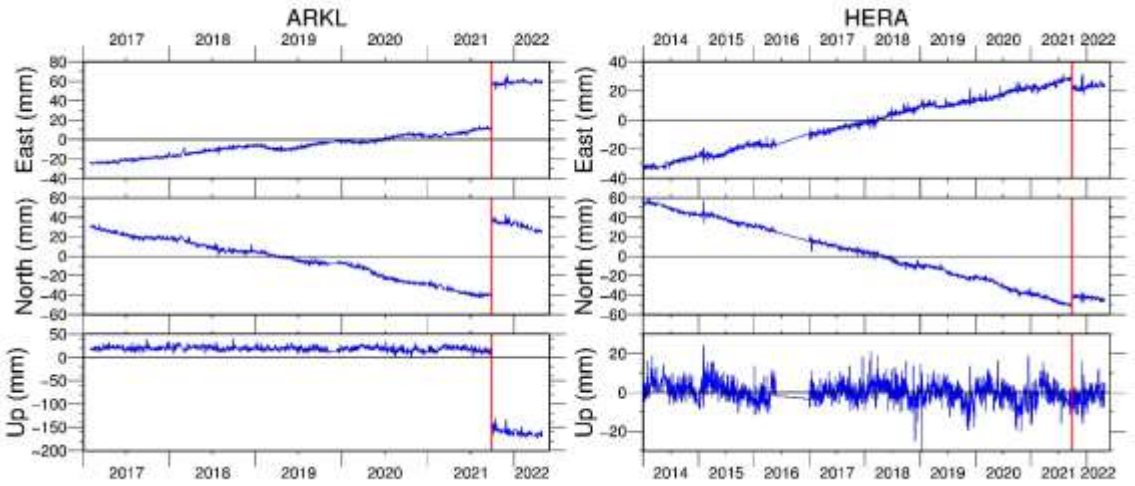

Figure S5. Time Series for GNSS sites ARKL and HERA. Red line indicates the strong Mw5.8 seismic event in Arkalochori village.

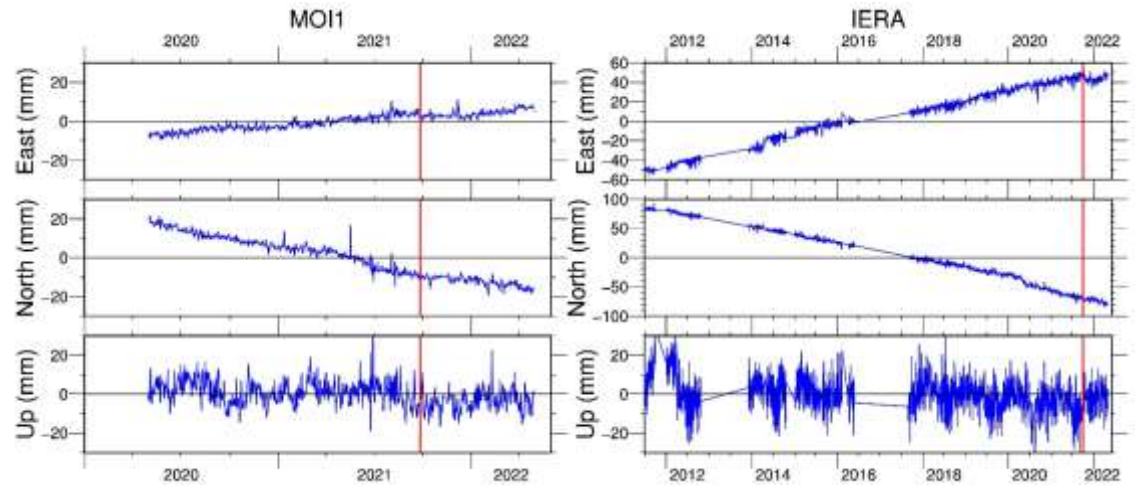

Figure S6. Time Series for GNSS sites MOI1 and IERA, located WSW and ESE from epicentral area, respectively. Red line indicates the September 27, 2021 earthquake